ACS APPLIED MATERIALS & INTERFACES

Research Article

www.acsami.org

Two-Dimensional Interface Engineering of a Titania–Graphene Nanosheet Composite for Improved Photocatalytic Activity

Jing Sun, Hui Zhang,* Liang-Hong Guo,* and Lixia Zhao

State Key Laboratory of Environmental Chemistry and Eco-toxicology, Research Centre for Eco-environmental Sciences, Chinese Academy of Sciences, 18 Shuangqing Road, P.O. Box 2871, Beijing 100085, China

Supporting Information

ABSTRACT: A graphene-based two-dimensional (2D) nanoplatform provides new opportunities for fabricating 2D heterojunction interfaces to fortify charge transfer in semiconductor assemblies. In this report, TiO_2 nanosheet/graphene composite based 2D–2D heterojunctions were fabricated by a solvothermal process. Microscopic and spectroscopic characterization revealed a homogeneous sheetlike morphology with intimate interfacial contact between the TiO_2 nanosheet and graphene due to chemical interactions. Compared with 0D–2D Degussa P25 (TiO_2)/graphene and 1D–2D TiO_2 nanotube/graphene composites, the 2D–2D TiO_2 nanosheet/graphene hybrid demonstrated higher photocatalytic activity toward the degradation of rhodamine B and 2,4-dichlorophenol under UV irradiation. Radical trapping and ESR experiments revealed the enhanced generation of ·OH and $O_2^{\bullet-}$ in the 2D–2D heterojunction system. By analyzing TiO_2 excited state deactivation lifetime, the interfacial electron transfer rates determined for 0D–2D, 1D–2D, and 2D–2D TiO_2/graphene composites were 1.15×10^8 s^{-1}, 3.47×10^8 s^{-1}, and 1.06×10^9 s^{-1}, respectively. It was therefore proposed that the fast charge separation in the TiO_2 nanosheet/graphene photocatalyst promoted the generation of reactive oxygen species and enhanced the photodegradation reactions. The results underscore the key role of nanomaterial dimensionality in interfacial charge transfer processes.

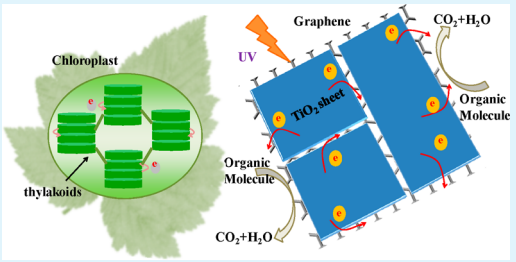

KEYWORDS: *photocatalysis, TiO_2 nanosheet, graphene, 2D–2D heterojunction, interfacial charge transfer*

INTRODUCTION

Sunlight-driven semiconductor photocatalysis has been receiving a great deal of attention due to its prominent ability in realizing solar energy conversion and environmental remediation.[1−3] The effectiveness of photocatalytic devices is dictated to a great extent by three processes: optical absorption, charge separation, and catalytic reaction on semiconductor surfaces. Among various photocatalysts, nanophase TiO_2 appears to be a suitable candidate because of its robust performance, low toxicity, low cost, and long-term stability.[4,5] By rationally engineering morphology, chemical composition, surface structure, and energy band, numerous photocatalytic applications for TiO_2 have been developed with tailored optoelectronic and catalytic properties.[6−9] However, the intrinsically fast recombination of charge carriers in their defect-rich bulk remains to be problematic.

Nanosized semiconductor heterojunction photocatalytic systems represent a typical strategy for enhancing charge carrier separation. The built-in electric field at the interface of the heterojunction can direct the flow of photogenerated charge carriers and thus inhibit the recombination process. In most cases, photogenerated electron transfer (ET) across the interface between the components is a key process in the heterogeneous catalytic system. Design of low-dimensional heterojunction interface (e.g., core/shell structured nanotube or nanorod architecture) has proved to be an effective way to promote charge carrier separation. For example, use of TiO_2 or carbon nanotubes as scaffolds has been developed to boost the photocatalytic performance of TiO_2-based systems.[10−12] Although these heterojunctions performed well in separating electron–hole pairs, further enhancement in interfacial ET to overcome electron transport limitation is highly desired to realize their full potential in practical photocatalytic settings.

The granum in green plants, which is composed of numerous thylakoids in a stacking structure with light-capturing molecules and electron transfer lumen, provides a valuable model for solar energy conversion. Inspired by the delicate structures and functional components in granum, a 2D–2D heterojunction structure would be helpful in achieving rapid charge transfer and separation in photocatalytic systems. The challenge in fabricating a 2D heterojunction system lies in developing a 2D platform for nanomaterial assembly to ensure continuous electron flow across the contacting interface. 2D flexible plane structure combined with excellent electron transport properties makes graphene an ideal platform for assembling heterojunction systems.[13−17] Previous studies have demonstrated enhanced photoelectrochemical performance of stacked TiO_2/graphene structure on solid substrates by a layer-by-layer

Received: September 11, 2013
Accepted: December 5, 2013
Published: December 5, 2013

assembly technique.[18,19] Such layered nanostructures are believed to increase the contact area between TiO_2 and graphene sheets and shorten the diffusion distance of photogenerated charge carriers, thus facilitating fast electron transfer across the heterojunction interface. However, the fabrication of a free-standing TiO_2/graphene 2D−2D structure is still a challenging task in photocatalytic applications. Moreover, the interfacial charge transfer reactions between graphene and different dimension TiO_2 are not completely understood. A better understanding of the effect of nanomaterial dimensionality on interfacial charge transfer processes is essential in the design of high-performance photocatalytic systems.

Herein, we constructed a TiO_2 nanosheet/graphene 2D−2D system with a well-defined heterojunction interface by a solvothermal method. Direct comparison with 0D−2D P25 (TiO_2)/graphene and 1D−2D TiO_2 nanotube/graphene hybrid nanomaterials was carried out in terms of photocatalytic degradation efficiency, reactive oxygen species (ROS) generation, and interfacial electron transfer kinetics. The key issue we would like to address is whether the TiO_2 nanosheet/graphene 2D−2D system, with its stacked structure and intimate interfacial contact, would promote the charge separation process after photoexcitation and eventually lead to more ROS generation and enhanced photocatalytic degradation activity.

EXPERIMENTAL SECTION

Chemicals. Graphite powder was purchased from Bodi Chemical Co. Ltd (Tianjin, China). Titanium(IV) fluoride (98%) was obtained from Alfa Aesar (Ward Hill, MA, USA). Degussa P25 and 2,4-dichlorophenol (2,4-DCP) were purchased from Sigma-Aldrich (St. Louis, MO, USA). Rhodamine B (RhB) and ethylenediaminetetraacetic acid disodium salt (EDTA-2Na) was purchased from Sinopharm Chemical Reagent Co., Ltd. (Shanghai, China). All other chemicals were of analytical reagent grade and used as received without further purification. Deionized water (resistance >18 MΩ cm) was prepared on a Millipore Milli-Q system (Bedford, MA, USA) and used throughout all experiments.

Preparation of TiO_2/Graphene Composites. Graphene oxide (GO) was prepared using a modified Hummers' method as detailed in the Supporting Information.[20−22] TiO_2 nanosheet/graphene composites were prepared by a solvothermal method. In a typical synthesis, 0.45 g of TiF_4 powder was sonicated in 20 mL of *n*-butanol and stirred for a few minutes to produce a homogeneous solution. Then, 0.9 mL of GO solution (1 g L^{-1}) in *n*-butanol was gradually added to the above solution and stirred for 0.5 h. After that, 0.14 mL of hydrofluoric acid (HF) was added dropwise into the solution with stirring. The above mixed solution was transferred into a 100 mL Teflon-lined autoclave immediately and maintained at 210 °C for 24 h in an oven. The resulting precipitates were separated by centrifugation, washed with ethanol and ultrapure water several times, and finally dried at 60 °C in an oven. The removal of fluorine was performed by treating the hybrids with 0.1 M NaOH solution

For comparison, a TiO_2 nanosheet sample was synthesized by a similar method without the addition of GO. A P25/graphene composite was prepared by a hydrothermal method according to the literature.[23] TiO_2 nanotube/graphene composites were prepared through an alkaline hydrothermal treatment.[24] The detailed synthesis procedures are described in the Supporting Information.

Characterization. The crystal structure of as-prepared products was measured by the powder X-ray diffraction (XRD) using X'Pert PRO MPD (Philips, Eindhoven, Netherlands) with Cu Kα radiation. The morphology and chemical composition were examined using an FEI Tecnai F20 S-TWIN transmission electron microscope (TEM) (Eindhoven, Netherlands) equipped with an energy-dispersive X-ray spectrometer (EDS). Atomic force microscopy (AFM) images were obtained on a Nanollla Multimode AFM (Digital Instrument Co., New York, NY, USA), operating in tapping mode with a scan rate of 1.20 Hz. Raman measurements were performed on a Renishaw inVia Raman spectroscope (Wotton-under-Edge, UK) with exciting wavelength at 532 nm. X-ray photoelectron spectroscopy (XPS) analysis was performed on a Thermo VG ESCALAB 250 spectrometer (East Grinsted, UK) with Al Kα X-ray radiation at 1486.6 eV. The background of the XPS peak was subtracted by Shirly subtraction and then deconvolved by Gaussian−Lorentzian shapes. An electron spin resonance (ESR) signal of the radicals spin trapped by 5,5-dimethyl-1-pyrroline-*N*-oxide (DMPO) was recorded on a JEOL JES FA200 X-band spectrometer (Tokyo, Japan) under photoirradiation with a 500 W mercury lamp (Ushio, USH 500D). The settings were the center field at 323.3 mT, microwave frequency at 9054.6 MHz, and power at 0.998 mW. A spectrofluorometer (Hitachi, F-4500) was used for the photoluminescence (PL) measurement at room temperature with an excitation wavelength at 375 nm. Photoluminescence lifetime decay was recorded on an Edinburgh Instruments F900 spectrometer (Livingston, UK) with a 375 nm laser excitation source and luminescence monitored at 430 nm.

Photocatalytic Degradation Experiments. Photocatalytic activities of the prepared catalysts were evaluated by the photodegradation of RhB and 2,4-DCP. Before irradiation, a suspension containing 60 mL of 10 mg L^{-1} RhB or 2,4-DCP and 0.04 g of the prepared photocatalyst was sonicated for 10 min and stirred for 30 min in the dark to ensure an adsorption/desorption equilibrium state. Then the above suspension was transferred into a cylindrical Pyrex glass reactor and illuminated with a 500 W tubelike high-pressure mercury lamp (Perfectlight Co Ltd., Beijing, China) with a maximum emission at approximately 365 nm. At a given time interval of irradiation, 2 mL aliquots were collected from the suspension and centrifuged. All the experiments were carried out under ambient conditions, and the temperature was maintained at 20 °C by recirculating a cooling water system. The residual concentration of RhB in the aliquot was analyzed by using an Agilent 8453 UV−vis spectrophotometer (Palo Alto, CA, USA). The concentration of 2,4-DCP was determined on a Waters 2695 high-performance liquid chromatograph (HPLC) (Milford, MA,USA) with an Agela Venusil MP C18 (0.46 μm × 250 mm) reverse-phase column equipped with a Waters 2996 photodiode array detector.

RESULTS AND DISCUSSION

Characterization of the TiO_2 Nanosheet/Graphene Composite. Graphene oxide was first synthesized and characterized. AFM images (Figure 1a) show that graphene oxide is two dimensional with an average height of 1.26 nm and lateral dimensions on the order of micrometers, suggesting successful exfoliation of graphite oxide down to single-layer or bilayer sheets. The oxidation process introduced oxygen-containing groups on the plane of the graphene oxide sheet,[24] providing anchoring sites for TiO_2 growth. TiO_2 nanosheet/graphene composites were synthesized by a simple solvothermal process to achieve in situ growth of the TiO_2 nanosheet on the graphene oxide sheet and simultaneous reduction of graphene oxide to graphene. Figure 1b demonstrates that the produced TiO_2 nanosheet is distributed uniformly on the graphene sheet and exhibits the two-dimensional sheetlike morphology. The nearly transparent feature of the TiO_2 sheet indicates its ultrathin thickness. This suggests the graphene sheet indeed acts as a 2D support for the growth of large TiO_2 nanosheets.

The homogenous combination of TiO_2 nanosheet/graphene composites is further confirmed by EDS analysis. Figure 1c−e displays the representative element mapping images of carbon and titanium in the hybrids. It demonstrates an even distribution of the two elements in the entire imaging area, reasonably indicating the homogeneous 2D−2D interfacial

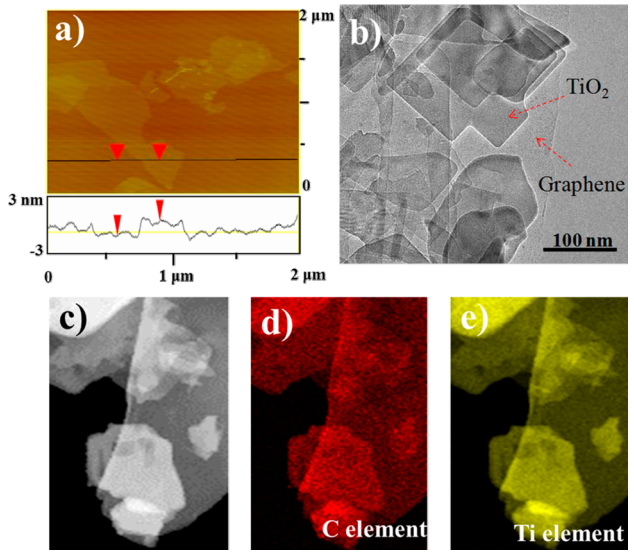

Figure 1. (a) Atomic force microcopy images of graphene oxide sheets. (b) Transmission electron microscopy images of TiO_2 nanosheet/graphene composites. (c–e) Element mapping images of TiO_2 nanosheet/graphene composites.

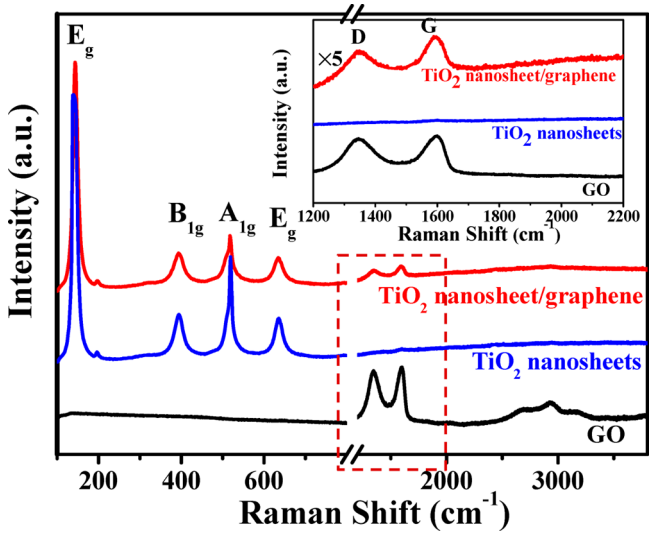

Figure 2. Raman spectra of graphene oxide, TiO_2 nanosheets, and TiO_2 nanosheet/graphene composites. The inset shows Raman spectra of the three nanomaterials in the 1200–2200 cm^{-1} region.

contact. These results indicate the realization of the 2D heterojunction interface in the TiO_2 nanosheet/graphene composites. The graphene content in the TiO_2 nanosheet/graphene composite is determined at ~2 wt % by the EDS analysis in Figure S1 (Supporting Information). In comparison, TEM images of P25/graphene (0D/2D) and TiO_2 nanotube/graphene (1D/2D) nanocomposites (Figure S2, Supporting Information) reveal the well-dispersed TiO_2 nanoparticle and nanotube on graphene sheet, respectively. To further investigate the morphology and structure of TiO_2 nanosheet/graphene composites, AFM images of the composites are conducted (Figure S3, Supporting Information). The TiO_2 nanosheet/graphene composites display a layer thickness with about 8–10 nm. Although the stacking style of the TiO_2 sheet and graphene in the composites cannot be examined, these results indicate the TiO_2 nanosheet anchors throughout the graphene sheet.

XRD patterns of the prepared samples are shown in Figure S4 (Supporting Information). The diffraction pattern of the TiO_2 nanosheet/graphene composite exhibits distinctive peaks of the pure anatase phase of TiO_2 (JCPDS No. 21-1272), which are similar to the diffraction peaks of the TiO_2 nanosheet alone. Notably, for the sample GO, the peak at $2\theta = 10.3^{\circ}$ corresponds to the (002) reflection of stacked GO sheets. However, no diffraction peak of GO is observed in the composites, attributing to the disruption of the GO layers.[25] The TiO_2 nanosheet anchored on the graphene surface is favorable for preventing the reduced GO from direct stacking after the solvothermal process. Such a pristine layer-by-layer assembly suggests the formation of a 2D heterojunction interface with high quality. Raman spectra provide additional insights into the local order of the products (Figure 2). The anatase phase of the TiO_2 nanosheet in the composites is further confirmed by the typical Raman bands at 153 cm^{-1} (E_g), 400 cm^{-1} (B_{1g}), 517 cm^{-1} (A_{1g}), and 640 cm^{-1} (E_g).[26] In addition, the D band centered at 1320 cm^{-1} (disorder band) and the G band at 1594 cm^{-1} (tangential vibration band) attributed to the graphene substrate are also present, indicating successful incorporation of graphene into the hybrids. The intensity ratios between D and G bands (I_D/I_G) reveal the relative concentration of defects or disorders (particularly the sp^3-hybridized defects) compared to the sp^2-hybridized graphene domains.[27−29] After the solvothermal process, the decrease of the I_D/I_G ratio from 0.91 to 0.83 implies the removal of hydroxyl and epoxy groups and the reduced defect density in the TiO_2 nanosheet/graphene composite.[28,29]

The interactions between the TiO_2 nanosheet and graphene in the hybrids are further investigated by XPS spectra. Figure 3a shows the Ti 2p XPS spectrum of TiO_2 nanosheet/graphene composites. Two bands centered at binding energies of 464.3 and 458.5 eV are assigned to Ti $2p_{1/2}$ and Ti $2p_{3/2}$ spin-orbital splitting photoelectrons in the Ti^{4+} oxidation state, respectively.[25,30] In addition, the separation between these two bands (5.8 eV) is in accordance with the chemical state of Ti^{4+} in the anatase TiO_2, which is consistent with XRD and Raman spectral data. Two peaks located at binding energies of 463.4 and 457.6 eV can be attributed to Ti^{3+} $2p_{1/2}$ and Ti^{3+} $2p_{3/2}$ peaks, indicating the existence of Ti^{3+} in addition to the Ti^{4+} oxidation state.[31] Besides, the bands at 465.2 and 459.4 eV of the Ti $2p_{1/2}$ and Ti $2p_{3/2}$ peaks are attributed to the formation of the Ti–C bond, suggesting the chemical interaction between TiO_2 nanosheets and graphene.[32]

The C 1s spectrum of GO can be deconvoluted into four peaks at binding energies of 284.5, 286.5, 287.1, and 288.8 eV, which are assigned to C–C, C–O, C═O, and O–C═O groups, respectively (Figure 3C).[29,33] These oxygen-containing bands on the surface of GO can act as anchoring sites for TiO_2 growth. After the solvothermal process, the XPS C 1s spectrum of TiO_2 nanosheet/graphene composites displays greatly reduced oxygen-containing groups, indicating the reduction of GO to graphene. It is noted that the deconvoluted peak centered at 283.7 eV is assigned to the Ti–C bond,[32,34] which is consistent with Ti 2p spectra in Figure 3a. In addition, a characteristic peak at 288.7 eV attributed to the Ti–O–C bond is also observed, indicating that the –OH group of the TiO_2 nanosheet possibly interacts with –COOH on the surface of graphene through an esterification reaction.[35,36] The binding energy at 529.6 eV in O 1s XPS spectra is closely related to the lattice oxide TiO_2, indicating the titanium atom bonds with

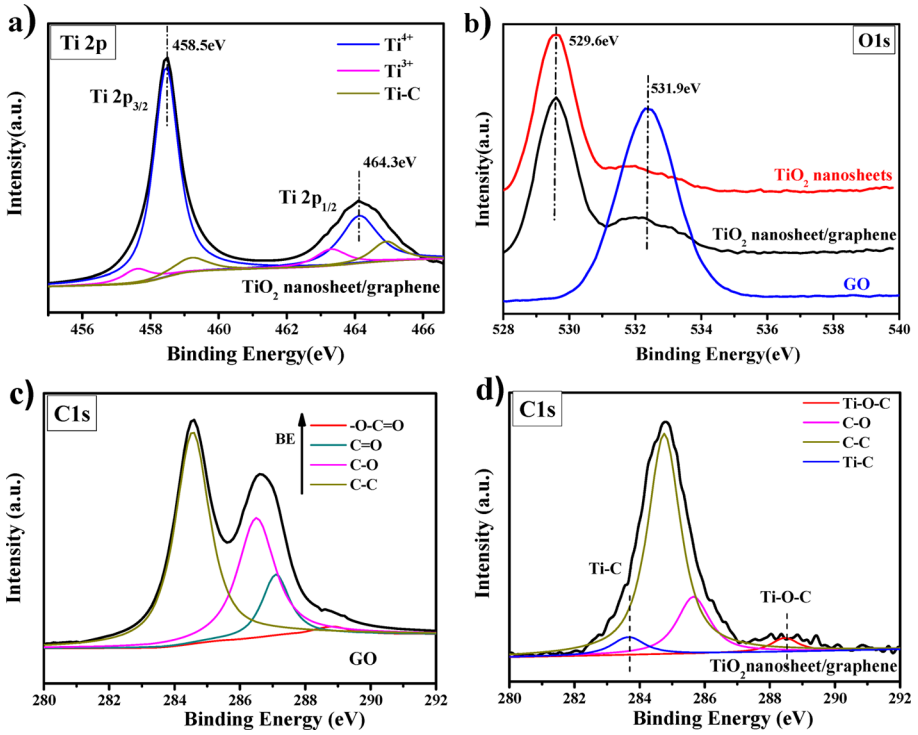

Figure 3. X-ray photoelectron spectroscopy results of the (a) Ti 2p band of TiO_2 nanosheet/graphene composites, (b) O 1s band of graphene oxide, TiO_2 nanosheets, and TiO_2 nanosheet/graphene composites, (c) C 1s band of graphene oxide, and (d) C 1s band of TiO_2 nanosheet/graphene composites.

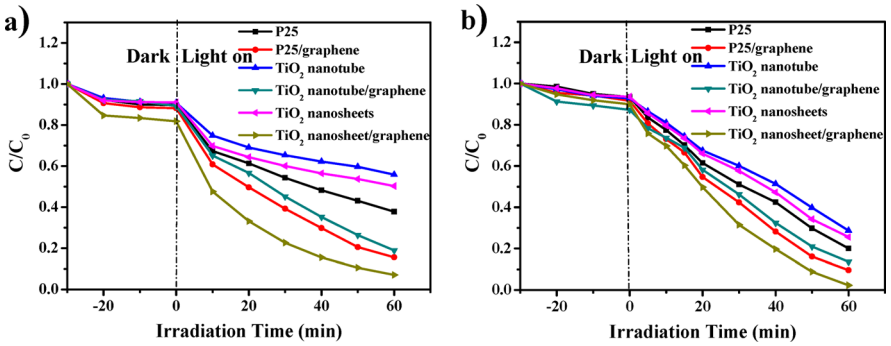

Figure 4. Photocatalytic degradation of (a) RhB and (b) 2,4-DCP over different photocatalysts under the irradiation of UV light. The time of light on is defined as 0 min. *C* represents the concentration of RhB or 2,4-DCP at time *t*, and C_0 stands for the initial solution.

oxygen rather than carbon. Binding energy at 531.9 eV is mainly attributed to the hydroxyl groups on the surface of GO.[37,38] The observation of both crystal lattice oxygen and hydroxyl groups in the synthesized material further demonstrates the existence of TiO_2 and graphene in the composite and intense interactions between the two components.

Photocatalytic Activity and Reaction Mechanism. Photocatalytic activity of the prepared samples was evaluated by photodegradation of RhB and 2,4-DCP under UV light. Figure S5 (Supporting Information) displayed the photocatalytic devices. For comparison, six different types of TiO_2 photocatalysts were examined, including P25 (0D), TiO_2 nanotube (1D), TiO_2 nanosheet (2D), P25/graphene (0D/2D), TiO_2 nanotube/graphene (1D/2D), and TiO_2 nanosheet/graphene (2D/2D). Figure 4a displays the temporal evolution of RhB concentration in the presence of the prepared photocatalysts. Adsorption of RhB on the nanomaterial reached an equilibrium state within 30 min in the dark. The control experiment displayed that few RhB molecules were degraded under UV light without photocatalyst (Figure S6, Supporting Information). Upon light irradiation, a sharp decrease of RhB concentration was observed on TiO_2 nanosheet/graphene samples, and approximately 95% of RhB dyes were degraded within 60 min, whereas about 80% of the dyes were bleached on P25/graphene and TiO_2 nanotube/graphene in the same reaction time. It needs to be noted that all three TiO_2/graphene composites exhibited higher photocatalytic activity compared with the corresponding pure TiO_2. This demonstrates that the heterojunction structure with incorporation of graphene contributed significantly to the photocatalytic activity of TiO_2. Interestingly, although the photocatalytic activity of pure TiO_2 nanosheets was slower than bare P25, the TiO_2 nanosheet/graphene displayed higher activity than P25/graphene. This suggests that the 2D−2D heterojunction structure is more beneficial to the photocatalyst than the other heterojunction structures. Similar results were obtained

with another degradation target 2,4-DCP, a commonly found environmental contaminant (Figure 4b). This indicates that TiO_2 nanosheet/graphene 2D heterojunction hybrids may be used as a universal photocatalyst for the elimination of organic pollutants.

The photodegration curves of RhB were fitted by pseudo-first-order reaction kinetics. The rate constant (k) was calculated to be 0.046 min^{-1} for the TiO_2 nanosheet/graphene composite and 0.0068 min^{-1} for the TiO_2 nanosheet, which exhibits almost seven-fold enhancement after graphene incorporation and only two-fold and five-fold enhancement for P25/graphene and TiO_2 nanotube/graphene, respectively. These experimental findings clearly demonstrate the important role of interfacial dimensionality in improving the photocatalytic performance.

It is commonly accepted that ROS produced in photocatalytic reactions usually govern the photocatalytic degradation processes.[39] To get more insight into the high photooxidation activity of TiO_2 nanosheet/graphene 2D−2D hybrids, the photocatalytic reaction was investigated by the radical trapping experiment. Figure S7 (Supporting Information) displays the degradation trace of RhB over P25/graphene, TiO_2 nanotube/graphene, and TiO_2 nanosheet/graphene with the addition of ROS scavengers. In all three photocatalytic systems, the RhB degradation process was greatly depressed by isopropanol (·OH scavenger) and EDTA-2Na (h^+ scavenger), verifying the important role of the ·OH and h^+ in the degradation process. It is worth noting that the TiO_2 nanosheet/graphene catalyst experienced a greater extent of suppression by *p*-benzoquinone than P25/graphene and TiO_2 nanotube/graphene. This strongly suggests that $O_2^{\bullet-}$ radical oxidation plays a significant role in the photocatalytic degradation of RhB over the TiO_2 nanosheet/graphene. This phenomenon may be associated with the efficient photogenerated electron transfer in the 2D heterojunction photocatalytic system, which facilitates more hole participation in the photocatalytic process and greatly promotes the oxygen molecules to yield $O_2^{\bullet-}$ radicals.[40,41] These produced $O_2^{\bullet-}$ radicals would further induce the formation of H_2O_2 and then participate in the photocatalytic processes.

The involvement of radical species is further confirmed by ESR experiments. In Figure 5, the signal intensity of DMPO−·OH species produced by TiO_2 nanosheet/graphene increased progressively under UV irradiation, suggesting the continuous generation of ·OH radicals. In contrast, the DMPO−·OH signal intensity in P25/graphene and TiO_2 nanotube/graphene suspensions increased in the first few minutes and subsequently decayed until barely discernible after 8 min irradiation (Figure S8a and S8c, Supporting Information). The decay of signal intensity is probably due to the photoinduced destruction of the DMPO−·OH adducts under UV irradiation that is faster than ·OH generation.[42] The steady signal observed with TiO_2 nanosheet/graphene indicates a higher generation rate of ·OH by the 2D/2D composite photocatalyst. The ESR signal of the DMPO−$O_2^{\bullet-}$ adduct displays a similar pattern of change as the DMPO−·OH adduct (Figure 5). In addition, methyl radical signals derived from ·OH radical reactions with DMSO were also observed, which is in accordance with the reported work.[43,44] These findings are consistent with the results of the radical trapping experiments.

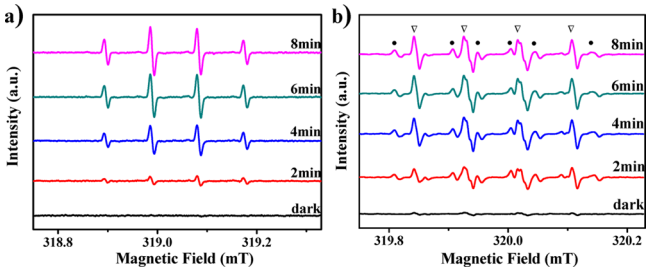

Figure 5. Electron spin resonance spectra of radical adducts trapped by DMPO in TiO_2 nanosheet/graphene dispersions as a function of time under UV irradiation: (a) DMPO−·OH formed in irradiated aqueous dispersions and (b) DMPO−$O_2^{\bullet-}$ formed in DMSO (DMPO−$O_2^{\bullet-}$ and methyl radical were marked with ∇ and ● symbols, respectively).

The stability of the photocatalyst was evaluated by performing the recycling experiments (Figure 6). No obvious decrease in the photodecomposition rate was observed after five cycles, indicating the nanocomposites exhibit relatively high stability during the photocatalytic degradation of pollutant molecules after a long time irradiation. In Figure S9 (Supporting Information), the XPS spectra of the TiO_2 nanosheet/graphene after five cycles of photodegradation experiments exhibited a slight decrease of the C−O peak, which is possibly due to the further photocatalytic reduction of the graphene in the TiO_2 nanosheet/graphene composites during the UV irradiation.[29,45] In addition, according to the previous report,[45] the carbon contents in the nanocomposites are possibly photodegradated by TiO_2 materials. However, these changes did not affect the photoactivity of the sample after long-term irradiation. These results indicate the photocatalytic performance of TiO_2 nanosheet/graphene composites is stable.

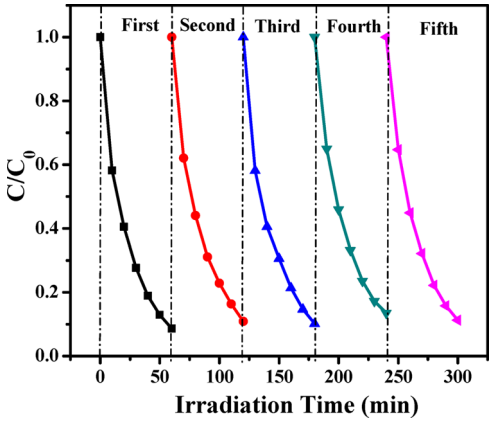

Figure 6. Five-cycle photocatalytic degradation of RhB over TiO_2 nanosheet/graphene composites.

Photoinduced Elecctron Transfer Dynamics. ROS generation during a photocatalytic reaction depends critically on the photo-induced generation of the electron−hole pair, electron transfer (ET) across the semiconductor interface, and electron−hole charge recombination.[3,46] An ET reaction that is faster than the charge recombination process is a key desideratum in improving photocatalytic efficiency. As a good electron acceptor, graphene could provide an efficient ET pathway for deactivating the excited state TiO_2.

The efficient charge separation and transfer in the TiO_2/graphene system can be supported by the steady state photoluminescence (PL) spectra. As shown in Figure S10

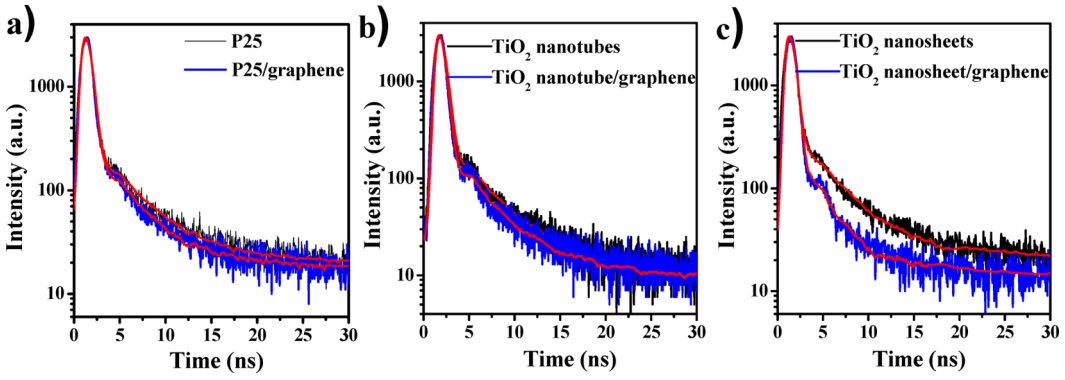

Figure 7. Photoluminescence decay curves of (a) P25 and P25/graphene, (b) TiO_2 nanotubes and TiO_2 nanotube/graphene, and (c) TiO_2 nanosheets and TiO_2 nanosheet/graphene in aqueous solutions with excitation wavelength at 375 nm and photoluminescence monitored at 430 nm.

(Supporting Information) the introduction of graphene quenched the PL intensity of excited TiO_2 nanostructures. Particularly, compared with the other two composites, TiO_2 nanosheet/graphene exhibited the most significantly diminished PL intensity, which demonstrates that the two-dimension heterojunction interface promotes the charge transfer more efficiently. This result is consistent with the highest photoreactivity of TiO_2 nanosheet/graphene composites.

Time-resolved photoluminescence was employed to further investigate the charge transfer dynamics across the TiO_2/graphene interface. Figure 7 shows the transient photoluminescence bleach decay of the prepared TiO_2/graphene composite, using the corresponding pure TiO_2 as the control. Previous studies have demonstrated that both the heterogeneity of samples and surface defects could introduce the multiexponential decay behavior of the charge recombination process.[47,48] The curves were fitted well to a biexponential decay function, with all the fitting parameters listed in Table 1.

Table 1. Kinetic Parameters of the Photoluminescence Decay Analysis of P25, P25/Graphene, TiO_2 Nanotubes, TiO_2 Nanotube/Graphene, TiO_2 Nanosheets, and TiO_2 Nanosheet/Graphene Composites[a]

photocatalyst	τ_1 (ns)	τ_2 (ns)	$a_1/(a_1 + a_2)$	$a_2/(a_1 + a_2)$	χ^2
P25	0.30	4.49	79.29%	20.71%	1.57
P25/graphene	0.29	3.92	83.17%	16.83%	1.38
TiO_2 nanotubes	0.36	4.52	82.53%	17.47%	1.56
TiO_2 nanotube/graphene	0.32	4.44	86.67%	13.33%	1.35
TiO_2 nanosheets	0.34	4.91	57.68%	42.32%	1.33
TiO_2 nanosheet/graphene	0.25	4.48	61.37%	38.63%	1.71

[a]The kinetic curve was fitted using a double exponential decay function given by $I(t) = b + a_1 \cdot \exp(-t/\tau_1) + a_2 \cdot \exp(-t/\tau_2)$.

For all three composite materials, incorporation of graphene reduced the photoluminescence lifetime of TiO_2, confirming the role of graphene in storing and shuttling electrons from photoexcited TiO_2 nanosheets. It was important to note that, compared with the corresponding bare TiO_2 samples, the fast time decay component (τ_1) in the TiO_2 nanosheet/graphene hybrid exhibited a greater decrease than P25/graphene and TiO_2 nanotube/graphene hybrids, suggesting a more efficient interaction and faster ET process in the 2D−2D heterojunction system. According to eq 1,[49] the apparent ET rate (k_{ET}) in P25/graphene, TiO_2 nanotube/graphene, and TiO_2 nanosheet/graphene hybrids is calculated to be 1.15×10^8 s^{-1}, 3.47×10^8 s^{-1}, and 1.06×10^9 s^{-1}, respectively.

$$k_{ET} = \frac{1}{\tau_1(TiO_2{-}RGO)} - \frac{1}{\tau_1(TiO_2)} \quad (1)$$

Compared with P25/graphene, an almost ten-fold enhancement of ET rate was achieved in the TiO_2 nanosheet/graphene based 2D−2D heterojunction system. It is believed that the 2D−2D heterojunction interface has more intimate physical and electronic coupling between TiO_2 and graphene, resulting in more effective ET quenching of the excited state TiO_2.

On the basis of the above results, the mechanisms for the enhanced photocatalytic degradation efficiency of the TiO_2 nanosheet/graphene system are proposed as follows. Due to the intimate and uniform contact between the two sheetlike nanomaterials in the composite photocatalyst, photogenerated electrons in the excited TiO_2 are injected rapidly into graphene across the 2D−2D heterojunction interface. Thus, effective charge separation between the electron−hole pair is achieved and leads to enhanced generation of ROS including ·OH and $O_2^{\bullet-}$ radicals. These radicals subsequently accelerate the oxidative degradation of RhB and 2,4-DCP.

CONCLUSIONS

0D−2D, 1D−2D, and 2D−2D TiO_2/graphene hybrids were synthesized and evaluated to provide fundamental insights into the photocatalytic enhancement mechanisms of nanocomposites. Due to the heterojunction interface nature of these hybrids, the TiO_2 nanosheet/graphene-based 2D−2D photocatalytic system possesses a stronger electronic and physical coupling effect, resulting in remarkable enhancement in the ET process and yielding superior photocatalytic activity toward contaminant degradation. This 2D−2D heterojunction system strategy offers a significant route to overcome carrier transfer limitation. This work could stimulate the development of a photocatalytic system with a well-defined nanocomposite interface to fulfill their potential in the photocatalytic devices.

ASSOCIATED CONTENT

Supporting Information

Synthesis of graphene oxide and TiO_2 nanotube/graphene hybrid, TEM images of P25/graphene and TiO_2 nanotube/graphene composites, XRD patterns, radical trapping experiment results, and ESR spectra of P25/graphene and TiO_2 nanotube/graphene composites. This material is available free of charge via the Internet at http://pubs.acs.org.

AUTHOR INFORMATION

Corresponding Authors

*Phone: 86 10-62849338. E-mail: huizhang@rcees.ac.cn (H.Z.).

*Phone: 86 10-62849685. E-mail: lhguo@rcees.ac.cn (L.-H.G.).

Notes

The authors declare no competing financial interest.

ACKNOWLEDGMENTS

This work was supported by the National Basic Research Program of China (2011CB936001, 2010CB933502) and National Nature Science Foundation of China (No. 21207146). We are indebted to Prof. Jingfu Liu, Dr. Rui Liu, and Dr. Junfang Sun at the Research Centre for Eco-environmental Sciences, Chinese Academy of Sciences for acquiring the Raman spectra.

REFERENCES

(1) Zou, Z. G.; Ye, J. H.; Sayama, K.; Arakawa, H. *Nature* **2001**, *414*, 625−627.

(2) Kamat, P. V. *J. Phys. Chem. C* **2007**, *111*, 2834−2860.

(3) Hoffmann, M. R.; Martin, S. T.; Choi, W. Y.; Bahnemann, D. W. *Chem. Rev.* **1995**, *95*, 69−96.

(4) Linsebigler, A. L.; Lu, G. Q.; Yates, J. T. *Chem. Rev.* **1995**, *95*, 735−758.

(5) Legrini, O.; Oliveros, E.; Braun, A. M. *Chem. Rev.* **1993**, *93*, 671−698.

(6) Wen, C. Z.; Zhou, J. Z.; Jiang, H. B.; Hu, Q. H.; Qiao, S. Z.; Yang, H. G. *Chem. Commun.* **2011**, *47*, 4400−4402.

(7) Liu, S. W.; Yu, J. G.; Jaroniec, M. *J. Am. Chem. Soc.* **2010**, *132*, 11914−11916.

(8) Hu, X.; Li, G.; Yu, J. C. *Langmuir* **2010**, *26*, 3031−3039.

(9) Burda, C.; Chen, X. B.; Narayanan, R.; El-Sayed, M. A. *Chem. Rev.* **2005**, *105*, 1025−1102.

(10) Jennings, J. R.; Ghicov, A.; Peter, L. M.; Schmuki, P.; Walker, A. B. *J. Am. Chem. Soc.* **2008**, *130*, 13364−13372.

(11) Kongkanand, A.; Dominguez, R. M.; Kamat, P. V. *Nano Lett.* **2007**, *7*, 676−680.

(12) Kuang, D.; Brillet, J.; Chen, P.; Takata, M.; Uchida, S.; Miura, H.; Sumioka, K.; Zakeeruddin, S. M.; Gratzel, M. *ACS Nano* **2008**, *2*, 1113−1116.

(13) Behnam, A.; Lyons, A. S.; Bae, M. H.; Chow, E. K.; Islam, S.; Neumann, C. M.; Pop, E. *Nano Lett.* **2012**, *12*, 4424−4430.

(14) Gilje, S.; Han, S.; Wang, M.; Wang, K. L.; Kaner, R. B. *Nano Lett.* **2007**, *7*, 3394−3398.

(15) Das, A.; Pisana, S.; Chakraborty, B.; Piscanec, S.; Saha, S. K.; Waghmare, U. V.; Novoselov, K. S.; Krishnamurthy, H. R.; Geim, A. K.; Ferrari, A. C.; Sood, A. K. *Nat. Nanotechnol.* **2008**, *3*, 210−215.

(16) Stankovich, S.; Dikin, D. A.; Dommett, G. H.; Kohlhaas, K. M.; Zimney, E. J.; Stach, E. A.; Piner, R. D.; Nguyen, S. T.; Ruoff, R. S. *Nature* **2006**, *442*, 282−286.

(17) Novoselov, K. S.; Geim, A. K.; Morozov, S. V.; Jiang, D.; Zhang, Y.; Dubonos, S. V.; Grigorieva, I. V.; Firsov, A. A. *Science* **2004**, *306*, 666−669.

(18) Kim, I. Y.; Lee, J. M.; Kim, T. W.; Kim, H. N.; Kim, H. I.; Choi, W.; Hwang, S. J. *Small* **2012**, *8*, 1038−1048.

(19) Tu, W.; Zhou, Y.; Liu, Q.; Tian, Z.; Gao, J.; Chen, X.; Zhang, H.; Liu, J.; Zou, Z. *Adv. Funct. Mater.* **2012**, *22*, 1215−1221.

(20) Hummers, W. S.; Offeman, R. E. *J. Am. Chem. Soc.* **1958**, *80*, 1339−1339.

(21) Cote, L. J.; Kim, F.; Huang, J. X. *J. Am. Chem. Soc.* **2009**, *131*, 1043−1049.

(22) Zhang, H.; Fan, X.; Quan, X.; Chen, S.; Yu, H. *Environ. Sci. Technol.* **2011**, *45*, 5731−5736.

(23) Zhang, H.; Lv, X. J.; Li, Y. M.; Wang, Y.; Li, J. H. *ACS Nano* **2010**, *4*, 380−386.

(24) Perera, S. D.; Mariano, R. G.; Vu, K.; Nour, N.; Seitz, O.; Chabal, Y.; Balkus, K. J. *ACS Catal.* **2012**, *2*, 949−956.

(25) Jiang, B.; Tian, C.; Pan, Q.; Jiang, Z.; Wang, J.-Q.; Yan, W.; Fu, H. *J. Phys. Chem. C* **2011**, *115*, 23718−23725.

(26) Zhang, H.; Xu, P.; Du, G.; Chen, Z.; Oh, K.; Pan, D.; Jiao, Z. *Nano Res.* **2010**, *4*, 274−283.

(27) Zhang, Y. H.; Tang, Z. R.; Fu, X.; Xu, Y. J. *ACS Nano* **2011**, *5*, 7426−7435.

(28) Liang, Y. T.; Vijayan, B. K.; Gray, K. A.; Hersam, M. C. *Nano Lett.* **2011**, *11*, 2865−2870.

(29) Akhavan, O. *ACS Nano* **2010**, *4*, 4174−4180.

(30) Mali, S. S.; Betty, C. A.; Bhosale, P. N.; Patil, P. S. *ECS J. Solid State Sci. Technol.* **2012**, *1*, M15−M23.

(31) Liu, H.; Yang, W.; Ma, Y.; Yao, J. *Appl. Catal. A: Gen.* **2006**, *299*, 218−223.

(32) Akhavan, O.; Azimirad, R.; Safa, S.; Larijani, M. M. *J. Mater. Chem.* **2010**, *20*, 7386.

(33) Liu, S. W.; Liu, C.; Wang, W. G.; Cheng, B.; Yu, J. G. *Nanoscale* **2012**, *4*, 3193−3200.

(34) Akhavan, O.; Abdolahad, M.; Abdi, Y.; Mohajerzadeh, S. *Carbon* **2009**, *47*, 3280−3287.

(35) Zhang, K.; Kemp, K. C.; Chandra, V. *Mater. Lett.* **2012**, *81*, 127−130.

(36) Liu, B.; Huang, Y.; Wen, Y.; Du, L.; Zeng, W.; Shi, Y.; Zhang, F.; Zhu, G.; Xu, X.; Wang, Y. *J. Mater. Chem.* **2012**, *22*, 7484.

(37) Liu, K. S.; Fu, H. G.; Shi, K. Y.; Xiao, F. S.; Jing, L. Q.; Xin, B. F. *J. Phys. Chem. B* **2005**, *109*, 18719−18722.

(38) Jiang, B.; Tian, C.; Wang, L.; Xu, Y.; Wang, R.; Qiao, Y.; Ma, Y.; Fu, H. *Chem. Commun.* **2010**, *46*, 4920−4922.

(39) Komaguchi, K.; Maruoka, T.; Nakano, H.; Imae, I.; Ooyama, Y.; Harima, Y. *J. Phys. Chem. C* **2009**, *113*, 1160−1163.

(40) Hirakawa, T.; Nosaka, Y. *Langmuir* **2002**, *18*, 3247−3254.

(41) Zhang, N.; Zhang, Y.; Pan, X.; Yang, M.-Q.; Xu, Y.-J. *J. Phys. Chem. C* **2012**, *116*, 18023−18031.

(42) Harbour, J. R.; Hair, M. L. *J. Phys. Chem.* **1979**, *83*, 652−656.

(43) Vaughan, P. P.; Blough, N. V. *Environ. Sci. Technol.* **1998**, *32*, 2947−2953.

(44) Eberhardt, M. K.; Colina, R. *J. Org. Chem.* **1988**, *53*, 1071−1074.

(45) Akhavan, O.; Abdolahad, M.; Esfandiar, A.; Mohatashamifar, M. *J. Phys. Chem. C* **2010**, *114*, 12955−12959.

(46) Du, J.; Lai, X. Y.; Yang, N. L.; Zhai, J.; Kisailus, D.; Su, F. B.; Wang, D.; Jiang, L. *ACS Nano* **2011**, *5*, 590−596.

(47) Robel, I.; Subramanian, V.; Kuno, M.; Kamat, P. V. *J. Am. Chem. Soc.* **2006**, *128*, 2385−2393.

(48) Lightcap, I. V.; Kamat, P. V. *J. Am. Chem. Soc.* **2012**, *134*, 7109−7116.

(49) Kongkanand, A.; Tvrdy, K.; Takechi, K.; Kuno, M.; Kamat, P. V. *J. Am. Chem. Soc.* **2008**, *130*, 4007−4015.